Multiple Measurement Vector Model for Sparsity-Based Vascular Ultrasound Imaging

Doğan , Didem; Kruizinga, Pieter; Bosch, Johannes G.; Leus, Geert

Multiple Measurement Vector Model for Sparsity-Based Vascular Ultrasound Imaging

Didem Dogan
Circuits and Systems Group
Delft University of Technology
Delft, The Netherlands
d.doganbaskaya@tudelft.nl

Pieter Kruizinga
Dept. of Neuroscience
Erasmus Medical Center
Rotterdam, The Netherlands
p.kruizinga@erasmusmc.nl

Johannes G. Bosch
Dept. of Biomedical Engineering
Erasmus Medical Center
Rotterdam, The Netherlands
j.bosch@erasmusmc.nl

Geert Leus
Circuits and Systems Group
Delft University of Technology
Delft, The Netherlands
g.j.t.leus@tudelft.nl

Abstract—Ultrasound imaging of the vasculature has major significance for the detection of cardiovascular diseases and cancer. However, limited spatial resolution or long acquisition times of existing techniques limit the visualization of the microvascular structures. Enforcing sparsity in the underlying vasculature as well as exploiting statistical independence between voxels have become prominent for fast super-resolution imaging. However, such a statistical independence may not be valid for all voxels and may hence lead to a distorted signal model. Here we present an image reconstruction method that exploits the sparsity of the vasculature data without distorting the original signal model. We employ a multiple measurement vector (MMV) model to enforce the joint sparsity over the images at different time instants. To reduce the computational complexity of obtaining the solution, the ℓ_1-SVD method is applied to the MMV model. We demonstrate that our method improves spatial resolution and provides a clear separation between blood vessels. Although our method is slightly slower than existing approaches, it outperforms them in terms of image reconstruction quality.

Index Terms—sparse reconstruction, vascular ultrasound imaging, multiple measurement vector (MMV) model, ℓ_1-SVD

I. INTRODUCTION

Ultrasound imaging is widely used in medicine as it is a non-invasive and cost-effective imaging technique [1]. Visualization of the vasculature has major significance for the detection of cardiovascular diseases and cancer. Cancer treatments cause structural changes in the microvascular structures, and hence exposing the microvasculature using ultrasound imaging can provide fast treatment [2]. However, fast detection of the hemodynamic changes over the microvasculature is prevented by spatial resolution limitations [3]. Therefore, there is a need for fast imaging methods that improve the spatial resolution of identifying the microvasculature structures.

Recently, sparse representations of signals [4], [5] have gained popularity in areas such as radar [6], magnetic resonance imaging (MRI) [7], and ultrasound imaging [8]. The specific regularization to solve the ultrasound imaging problem is the sparse structure of the vascular network [3]. A signal is sparse if it can be represented by a vector with most coefficients zero, in an appropriate transform domain [9].

Here we focus on the sparsity-based ultrasound hemodynamic imaging problem presented in [3], [10]. A method

named SUSHI has been developed to improve the spatial resolution in contrast-enhanced ultrasound imaging. It is a fast method exploiting sparsity in the correlation domain of the underlying vasculature structure [11], [12]. This method assumes that the temporal fluctuations in volume cells that belong to different vessels are statistically independent [3].

In this work, we propose an image reconstruction method that directly uses the sparse structure of the vasculature instead of enforcing sparsity in the correlation domain. Although assuming statistical independence between the flows in different vessels is computationally advantageous, this assumption ignores that blood cells from the same vessel are correlated to each other. Here we aim to avoid such a statistical independence assumption. Since the vasculature at different time instants does not change considerably, we on the other hand exploit the temporal correlation of the frames to improve the spatial resolution. For this, we employ a multiple measurement vector (MMV) model and enforce the joint sparsity of the vasculature in different frames [13]. Note that such a joint sparsity problem can be considered as a group lasso problem, with ℓ_1-relaxation [14]. Furthermore, the number of measurements can be decreased using the ℓ_1-SVD method thereby reducing the computational complexity of solving the MMV problem [15].

The remainder of this work is organized as follows. In the next section, we define the signal model for the ultrasound imaging problem of the vasculature. In Section III, we present the inverse problem by incorporating the available joint sparsity information. In Section IV, we express the steps of the optimization method that solves the inverse problem. Then, we comparatively evaluate the performance of the proposed method with the state-of-the-art. In the final section, we discuss the results and conclude this work.

II. FORWARD MODEL

In this section, we introduce the problem and relate our proposed approach to an existing method from literature. In ultrasound imaging, we first construct the image formation model and represent this in the form of a matrix-vector multiplication. For simplicity, we consider an imaging model for a system with a single transmitter that transmits a series of pulses. However, the model can easily be extended to multiple

transmitters. At every period Δt a pulse $a(t)$ is sent, where t is assumed to be continuous time and the peak of the pulse is assumed to be located at $t = 0$. At sensor n and pulse period m, the sensor output is modeled as

$$
\begin{aligned}
x(n, t, m) &= \sum_{x,z} a_{n,t}(x, z) \sum_v f(x, z, v) \exp^{jvm\Delta t} \\
&= \sum_{x,z} a_{n,t}(x, z) s(x, z, m),
\end{aligned}
\tag{1}
$$

where $f(x, z, v)$ is the total amount of scattering of all blood cells in a high resolution volume cell centered at position (x, z) and radial velocity v. Note that $a_{n,t}(x, z) = a(t - \tau_{x,z,n})$, where $\tau_{x,z,n}$ is the delay related to the distance from the transmitter to the receiver n through the pixel at (x, z). Lastly, $s(x, z, m)$ is the time-varying scattering signal related to the position (x, z).

In commercial ultrasound imaging, users generally only have access to the beamformed data. Applying delay-and-sum (DAS) beamforming on $x(n, t, m)$ from (1) at a low resolution with spacing (Δ_x, Δ_z), the output of the DAS beamformer for the low-resolution pixel at position (k, l) and pulse period m is given by

$$
\begin{aligned}
z(k, l, m) &= \sum_n x(n, \tau_{k\Delta_x, l\Delta_z, n}, m) \\
&= \sum_n \sum_{x,z} a(\tau_{k\Delta_x, l\Delta_z, n} - \tau_{x,z,n}) s(x, z, m) \\
&= \sum_{x,z} h_{k,l}(x, z) s(x, z, m),
\end{aligned}
\tag{2}
$$

where $h_{k,l}$ is assumed to be the point spread function (PSF) of the imaging system. Note that instead of a DAS, a matched filter can also be used as beamformer for the above formulation. In literature, several works assume $h_{k,l}$ as a shift-invariant point spread function [16], [17], but this assumption generally does not hold for realistic systems.

After obtaining $z(k, l, m)$ in (2), several preprocessing steps are performed on $z(k, l, m)$ prior to performing sparse reconstruction. First, a singular value decomposition (SVD) is applied to separate the tissue and blood flow subspaces and we obtain the blood related part $y(k, l, m)$ [18]. Sparsity will only be enforced over the blood flow subspace. Subsequent to SVD filtering, the phase of the received signal is manipulated to separate different flows (in terms of direction and/or speed) with Doppler processing. This separation is expected to provide additional anatomical information and a sparser structure compared to the original signal [3]. A bank of B bandpass filters is applied to $y(k, l, m)$ to obtain different videos with different velocities:

$$
y^{(b)}(k, l, m) = \sum_{x,z} h_{k,l}(x, z) s^{(b)}(x, z, m).
\tag{3}
$$

For $B = 2$, the blood flow is separated into a positive and negative flow, which corresponds to positive and negative frequencies in the Doppler domain. Note that this filterbank is not crucial and we will not use it for all our experiments. To simplify the presentation, in the remainder of this paper, we will drop the superscript b but keep in mind that the presented models and methods apply to any of the frequency bands.

Some approaches such as SUSHI assume that the signal fluctuations in volume cells that belong to different blood vessels are statistically independent [3], [10]. With this assumption, the autocorrelation of the beamformed and preprocessed measurements $y(k, l, m)$ in (3) can be approximated as

$$
r_y(k, l) = \sum_m |y(k, l, m)|^2 \approx \sum_{x,z} |h_{k,l}(x, z)|^2 r_s(x, z),
\tag{4}
$$

where $r_s(x, z) = \sum_m |s(x, z, m)|^2$. In (4), the cross-correlation terms are ignored as the signals from different vessels are assumed uncorrelated. Signals from pixels that are in the same vessel are not uncorrelated, but for those signals the cross terms are still dropped since they are not deemed important for obtaining super-resolution imaging. Notice how the approximation results in a squared absolute-valued PSF, which is narrower than the original PSF and therefore provides improved separation between vessels [3]. Although this approach has some clear advantages, we want to investigate some techniques that do not distort the original signal model of (3). Therefore, we propose not to solve the problem in the correlation domain and directly work with the original signal model in (3).

While (4) is based on a single measurement vector (SMV) model in the correlation domain [3], we employ an MMV model based on (3) which exploits different pulse periods in synergy [13], [15]. Such an MMV model is obtained by stacking the $y(k, l, m)$ and $s(x, z, m)$ values respectively into a space-time matrix $\mathbf{Y}$ and $\mathbf{S}$, resulting in the model

$$
\mathbf{Y} = \mathbf{HS} + \mathbf{N},
\tag{5}
$$

where the $\mathbf{H}$ matrix contains $h_{k,l}(x, z)$. Here $\mathbf{Y} = [\mathbf{y}_1 ... \mathbf{y}_M]$ and $\mathbf{S} = [\mathbf{s}_1 ... \mathbf{s}_M]$ represent a horizontal concatenation of respectively the vectorized measurements $\mathbf{y}_m$ and unknown images $\mathbf{s}_m$ related to the mth pulse period. Note that $\mathbf{y}_m$ and $\mathbf{s}_m$ include vertically concatenated elements of $s(x, z, m)$ and $y(k, l, m)$ for a particular m. Finally, $\mathbf{N}$ is similarly defined as $\mathbf{Y}$ and represents additional noise that is picked up at the receiving elements.

III. INVERSE PROBLEM

In the inverse problem, the goal is to recover the unknown images, $\mathbf{S}$, from their noisy and distorted measurements, $\mathbf{Y}$. Here, the image data is reconstructed by combining information from the measurements with some additional prior (statistical or structural) knowledge about the unknown image data. The sparsity-based MMV image reconstruction problem is formulated as

$$
\min_{\mathbf{S}} \ \frac{1}{2} ||\mathbf{Y} - \mathbf{HS}||_F^2 + \lambda ||\mathbf{S}||_{2,1}
\tag{6}
$$

where the $\ell_{2,1}$-norm is the sparse regularizer enforcing the joint sparsity of the image over different time instants [15]. In the matrix $\mathbf{S}$, the sparsity is enforced only in the spatial domain as the signal is not sparse over the time dimension. Since the vasculature at different time instants is similar, we expect that all columns have the same sparsity pattern. As a result, we exploit the temporal correlation to obtain a better spatial resolution. This is referred to as joint (or group) sparsity in the literature [19] and it can be enforced via the $\ell_{2,1}$-norm. We first compute the ℓ_2-norm of all rows of $\mathbf{S}$.
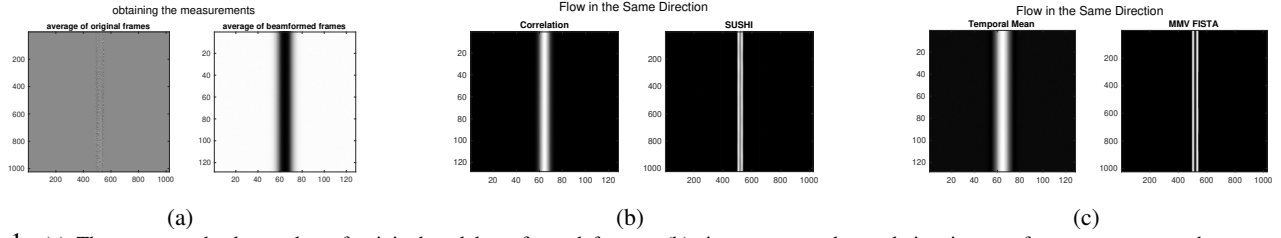
Fig. 1: (a) The average absolute value of original and beamformed frames, (b) tissue separated correlation image of measurements and reconstructed correlation image with SUSHI, and (c) temporal mean of tissue separated measurements and reconstructed image with MMV FISTA

Then, we construct the $\mathbf{s}^{(\ell_2)}$ vector, which stacks the ℓ_2-norms of the rows of $\mathbf{S}$. Finally, $||\mathbf{S}||_{2,1} = ||\mathbf{s}^{(\ell_2)}||_1$ is computed [15].

The main disadvantage of the MMV model is computational complexity. To reduce this cost, the number of measurements is decreased via the SVD, which relies on the fact that the set of vectors $\{\mathbf{y}_m\}_{m=1}^M$ lies in a P-dimensional subspace with $P \ll M$. To find this subspace, we first take the SVD of $\mathbf{Y}$ resulting in $\mathbf{Y} = \mathbf{ULV}^T$. Then a reduced matrix which contains most of the signal power is obtained as $\tilde{\mathbf{Y}} = \mathbf{ULD}_P = \mathbf{YVD}_P$ where $\mathbf{D}_P = [\mathbf{I}_P \ \mathbf{0}]^T$. Similary, we multiply $\mathbf{S}$ and $\mathbf{N}$ by these matrices and obtain $\tilde{\mathbf{S}} = \mathbf{SVD}_P$ and $\tilde{\mathbf{N}} = \mathbf{NVD}_P$. Now, instead of the large problem in (6) we solve the following problem

$$\min_{\tilde{\mathbf{S}}} \frac{1}{2}||\mathbf{H}\tilde{\mathbf{S}} - \tilde{\mathbf{Y}}||_F^2 + \lambda||\tilde{\mathbf{S}}||_{2,1}, \qquad (7)$$

whose solution can be obtained faster. This approach is known at the ℓ_1-SVD method. If the model does not contain any noise and the signal subspace has exactly order P, the solutions of (6) and (7) are the same, i.e. $\tilde{\mathbf{S}} = \mathbf{S}$. In case of noise, the approach in (7) also has a denoising effect. Finally, note that the SVD was already adopted in the preprocessing stage and hence the SVD required to formulate (7) does not introduce any additional complexity.

IV. Image Reconstruction Method

The optimization problem (7) can now be solved using any off-the-shelf solvers for MMV inverse problems [20]. M-FOCUSS and standard sparse Bayesian learning (SBL) include a large inverse and thus are computationally complex for large-scale problems [21], [22]. On the other hand, inverse-free SBL [23], ADMM [24] and FISTA [20] do not include

---

Output: $\mathbf{S}$: vectorized unknown images
Input: $\tilde{\mathbf{Y}}$: vectorized measurements, $\mathbf{H}$: sensing matrix, K: number of iterations
Initialize $\lambda > 0$, $L_f = ||\mathbf{H}^H\mathbf{H}||_2$, $t_1 = 1$, $\tilde{\mathbf{S}}_0 = \mathbf{Z}_1$, $k = 1$
while $k < K$ **do**
  calculate $\mathbf{Q}_k = \mathbf{Z}_k - \frac{1}{L_f}(\mathbf{H}^H\mathbf{H}\mathbf{Z}_k - \mathbf{H}^H\tilde{\mathbf{Y}})$
  compute $\tilde{S}_k^{(i,j)} = Q_k^{(i,j)}(1 - \frac{\lambda}{||\mathbf{Q}_k^{(i)}||_2})$ where $Q_k^{(i,j)}$
  is (i,j)th element of $\mathbf{Q}_k$ matrix and $\mathbf{Q}_k^{(i)}$ is the ith row of $\mathbf{Q}$ matrix
  update $t_{k+1} = 0.5(1 + \sqrt{1 + 4t_k^2})$
  update $\mathbf{Z}_{k+1} = \tilde{\mathbf{S}}_k + \frac{t_{k-1}}{t_{k+1}}(\tilde{\mathbf{S}}_k - \tilde{\mathbf{S}}_{k-1})$
  end
$\mathbf{S} = \tilde{\mathbf{S}}_K\mathbf{D}_P^T\mathbf{V}^T$

Algorithm 1: MMV FISTA

---

a large inverse and hence allow for a fast solution. However, for a fair comparison with SUSHI, which solves the problem using FISTA, we apply the MMV version of FISTA whose updating steps for solving (7) are given in Algorithm 1 [25]. Finally, note that $\mathbf{S}$ is easily obtained from $\tilde{\mathbf{S}}$ using a simple matrix product. In MMV FISTA, the computational complexity in each iteration is $\mathcal{O}(N^2P)$ where $s(x, z, m)$ has N pixels for the mth frame; however, SUSHI has a complexity of $\mathcal{O}(N^2)$.

V. Numerical Results

In this section, we comparatively evaluate the performance of the developed method with SUSHI for two scenarios [3].

A. Results with Shift-Invariant Sensing Matrix

In this section, we use a shift-invariant $\mathbf{H}$ matrix in (5) although the shift-invariancy assumption for the sensing matrix generally does not hold. Note that the sensing matrix for the SUSHI based on the model in (4) is equal to the element-wise square of the $\mathbf{H}$ matrix. The shift-invariant matrix-vector multiplication in (5) corresponds to a convolution with the point spread function (PSF) in the spatial domain, and hence to an element-wise multiplication in the spatial frequency domain. Therefore, both SUSHI and our method are implemented efficiently in the frequency domain. Here, we use the PSF from [3] to compare the different algorithms.

For the first simulation, we used 101 frames containing two parallel blood vessels where the blood flows in the same direction, represented by $s(x, z, m)$, for $m = 1, 2, ..., 101$. The high-resolution frames are of size 1024×1024 and their average absolute value is shown in Fig. 1a. The background
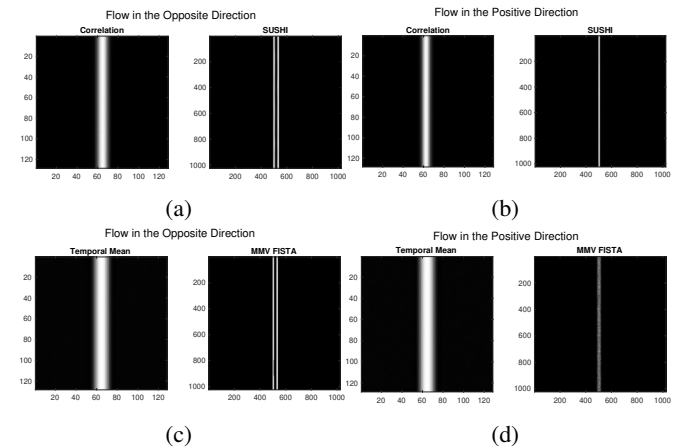

Fig. 2: (a),(b) Tissue separated and reconstructed images with SUSHI, and (c),(d) temporal mean of tissue separated and reconstructed images with MMV FISTA
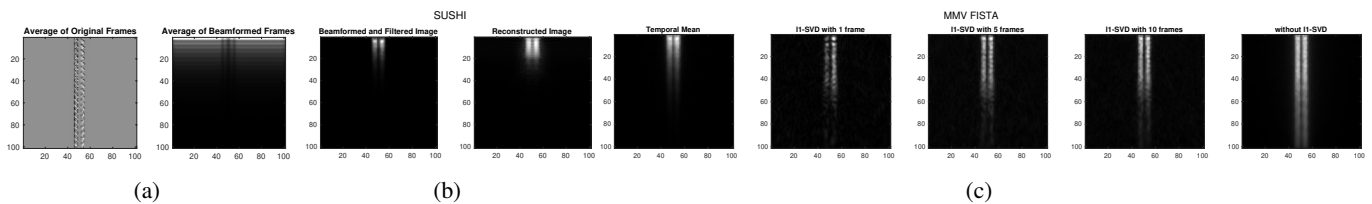
Fig. 3: (a) The average absolute value of original and beamformed frames, (b) tissue separated and reconstructed correlation images with SUSHI, (c) temporal mean of tissue separated images and reconstructed images with MMV FISTA when 101 frames are reduced to 1, 5 and 10 frames, and all frames are used

is assumed to have an intensity of 1000 whereas the blood flow has an intensity of $1000 + 30 \times \mathcal{N}(0,1)$. Here, the low-resolution beamformed images $z(k, l, m)$, are of size 128×128. White Gaussian noise with 20 dB SNR is added to the measurements. After obtaining $z(k, l, m)$, which is also displayed in Fig. 1a, the tissue is separated from the blood flow by using SVD filtering and keeping only the components related to the blood flow as $y(k, l, m)$. Since the flow direction is the same, Doppler processing is not considered here.

For SUSHI, the correlation image $r_y(k, l)$ consists of a single frame as shown in Fig. 1b. The temporal mean of the tissue separated image $y(k, l, m)$ is also given in Fig. 1c. To reduce the number of frames to a single frame in the MMV model, the ℓ_1-SVD is applied with $P = 1$. Since we only have a simple image and a well-conditioned sensing matrix of the PSF, a single frame is sufficient. Note though that the ℓ_1-SVD may require more frames for complex structures such as actual vasculature. We further select $\lambda = 0.5$ in (7) for 20 dB SNR. The reconstructions with SUSHI and MMV FISTA are shown in Fig. 1b and 1c, respectively. Here, we plot the reconstructed $r_s(x, z)$ in (4) for SUSHI and the temporal mean of the reconstructed $s(x, z, m)$ in (3) for the MMV FISTA. Although their image reconstruction times are the same for this simulation, the MMV FISTA algorithm outperforms SUSHI. Fig. 1b shows that SUSHI could not separate the blood vessels as they are very close to each other and their flow is correlated.

For the second simulation, we use the same setting but this time the synthetic flow moves downward in the right vessel and upward in the left one. We consider a simulation with and without Doppler processing to separate positive and negative flow. Both algorithms perform similarly for the opposing flow image (without Doppler processing) and the positive flow image (with Doppler processing) in Fig 2. Since the flow in the different vessels is uncorrelated now, SUSHI (with and without Doppler processing) can separate the vessels.

B. Results with Sensing Matrix Obtained from k-Wave

In this section, instead of using a simulated shift-invariant $\mathbf{H}$ matrix, the image reconstruction is performed with a realistic sensing matrix. Here, we assume matched filter beamforming for $\mathbf{X} = \mathbf{AS} + \mathbf{W}$, where $\mathbf{X}$ corresponds to the sensor measurements of the ultrasound imaging system (1). Using the matched filter $\mathbf{A}$, we can obtain the system in (2), $\mathbf{Z} = \mathbf{A}^H \mathbf{X} = \mathbf{A}^H \mathbf{AS} + \mathbf{N} = \mathbf{HS} + \mathbf{N}$, with $\mathbf{H} = \mathbf{A}^H \mathbf{A}$, which is not a shift-invariant matrix. Here, $\mathbf{A}$ is constructed using the k-wave toolbox in MATLAB for an imaging system with 128 transmitters and receivers [26] [27].

Furthermore, the $\mathbf{A}$ matrix is constructed in the frequency domain instead of the time domain. The advantage of a frequency-domain implementation is that number of frequency samples is smaller than the number of time samples, and it provides fast beamforming [28]. Since the sensing matrix is not shift-invariant, a fast multiplication with $\mathbf{H}$ cannot be performed.

For these simulations, we use the same setting as in the second simulation of Section V-A with opposing flow. However, both $s(x, z, m)$ and $z(k, l, m)$ in Fig. 3a are now of size 101×101. Therefore, we do not solve a super-resolution problem but a simple image reconstruction problem. Note that, even though $\mathbf{H}$ is a square matrix, the system is still highly ill-posed and requires regularization. The tissue is separated from the blood flow by using SVD filtering to obtain $y(k, l, m)$ but no Doppler processing is considered here.

The tissue separated correlation image $r_y(k, l)$ and the SUSHI reconstruction $r_s(x, z)$ are shown in Fig. 3b. The number of frames are reduced to 1, 5 and 10 using the ℓ_1-SVD method for the reconstructions with MMV FISTA. Finally, the full set of frames are used. The temporal mean of the tissue separated images $y(k, l, m)$ and recovered images $s(x, z, m)$ are displayed in Fig. 3c for several cases. When a single frame is used, the image reconstruction performance of SUSHI and MMV FISTA are similar. Still, the bottom part of the image is more visible with MMV FISTA. Since SUSHI squares the sensing matrix and the reconstructed image in the forward model, high-intensity parts become stronger, and low-intensity parts weaken. The image reconstruction performance of our method improves with an increasing number of frames. Each iteration of SUSHI and MMV FISTA with a single frame takes 0.04 seconds. Each iteration of MMV FISTA with 5, 10, and all frames takes 0.05, 0.06, and 0.2 seconds, respectively. Therefore, increasing the number of frames does not cause a huge increase in the computational time of the MMV FISTA algorithm.

VI. CONCLUSIONS AND DISCUSSION

In this work, we have proposed an image reconstruction method that directly exploits the joint sparse structure of the vasculature. To reduce the computational complexity, the ℓ_1-SVD algorithm is performed over the measurements. We evaluated the performance of our method within two different simulation settings. In the first set of experiments, we have demonstrated that our method improves the spatial resolution and provides a clear separation between very close vessels. For the second set of more realistic experiments, our method seems slightly slower than SUSHI but its image reconstruction quality is better under appropriate settings.

REFERENCES

[1] P. Kruizinga, P. van der Meulen, A. Fedjajevs, F. Mastik, G. Springeling, N. de Jong, J. G. Bosch, and G. Leus, "Compressive 3d ultrasound imaging using a single sensor," *Science Advances*, vol. 3, no. 12, 2017.

[2] R. K. Jain, "Normalization of tumor vasculature: An emerging concept in antiangiogenic therapy," *Science*, vol. 307, no. 5706, pp. 58–62, 2005.

[3] A. Bar-Zion, O. Solomon, C. Tremblay-Darveau, D. Adam, and Y. C. Eldar, "Sushi: Sparsity-based ultrasound super-resolution hemodynamic imaging," *IEEE Transactions on Ultrasonics, Ferroelectrics, and Frequency Control*, vol. 65, no. 12, pp. 2365–2380, 2018.

[4] Y. C. Eldar, *Sampling Theory: Beyond Bandlimited Systems*. Cambridge University Press, 2015.

[5] M. Elad, *Sparse and Redundant Representations: From Theory to Applications in Signal and Image Processing*, 1st ed. Springer Publishing Company, Incorporated, 2010.

[6] R. Baraniuk and P. Steeghs, "Compressive radar imaging," in *2007 IEEE Radar Conference*, 2007, pp. 128–133.

[7] M. Lustig, D. Donoho, and J. M. Pauly, "Sparse mri: The application of compressed sensing for rapid mr imaging," *Magnetic Resonance in Medicine*, vol. 58, no. 6, pp. 1182–1195, 2007.

[8] T. Chernyakova and Y. C. Eldar, "Fourier domain beamforming: The path to compressed ultrasound imaging," 2013.

[9] E. J. Candes, J. Romberg, and T. Tao, "Robust uncertainty principles: Exact signal reconstruction from highly incomplete frequency information," *IEEE Trans. Inf. Theor.*, vol. 52, no. 2, p. 489–509, Feb. 2006.

[10] A. Bar-Zion, C. Tremblay-Darveau, O. Solomon, D. Adam, and Y. C. Eldar, "Fast vascular ultrasound imaging with enhanced spatial resolution and background rejection," *IEEE Transactions on Medical Imaging*, vol. 36, no. 1, pp. 169–180, 2017.

[11] D. Cohen and Y. C. Eldar, "Sub-nyquist sampling for power spectrum sensing in cognitive radios: A unified approach," *IEEE Transactions on Signal Processing*, vol. 62, no. 15, pp. 3897–3910, 2014.

[12] P. Pal and P. P. Vaidyanathan, "Pushing the limits of sparse support recovery using correlation information," *IEEE Transactions on Signal Processing*, vol. 63, no. 3, pp. 711–726, 2015.

[13] J. Yang, A. Bouzerdoum, F. H. C. Tivive, and M. G. Amin, "Multiple-measurement vector model and its application to through-the-wall radar imaging," in *2011 IEEE International Conference on Acoustics, Speech and Signal Processing (ICASSP)*, 2011, pp. 2672–2675.

[14] A. Rakotomamonjy, "Surveying and comparing simultaneous sparse approximation (or group-lasso) algorithms," *Signal Processing*, vol. 91, no. 7, pp. 1505–1526, 2011.

[15] D. Malioutov, M. Cetin, and A. Willsky, "A sparse signal reconstruction perspective for source localization with sensor arrays," *IEEE transactions on signal processing*, vol. 53, no. 8, pp. 3010–3022, 2005.

[16] C. Dalitz, R. Pohle-Fröhlich, and T. Michalk, "Point spread functions and deconvolution of ultrasonic images," *IEEE transactions on ultrasonics, ferroelectrics, and frequency control*, vol. 62, pp. 531–544, 03 2015.

[17] H.-C. Shin, R. Prager, J. Ng, H. Gomersall, N. Kingsbury, G. Treece, and A. Gee, "Sensitivity to point-spread function parameters in medical ultrasound image deconvolution," *Ultrasonics*, vol. 49, no. 3, p. 344—357, March 2009.

[18] J. Baranger, B. Arnal, F. Perren, O. Baud, M. Tanter, and C. Demené, "Adaptive spatiotemporal svd clutter filtering for ultrafast doppler imaging using similarity of spatial singular vectors," *IEEE Transactions on Medical Imaging*, vol. 37, no. 7, pp. 1574–1586, 2018.

[19] S. Huang, H. Zhang, and A. Pižurica, "Joint sparsity based sparse subspace clustering for hyperspectral images," in *IEEE Conference on International Conference on Image Processing (ICIP)*, Athens, Greece, October 2018, pp. 3878–3882.

[20] A. Beck and M. Teboulle, "A fast iterative shrinkage-thresholding algorithm for linear inverse problems," *SIAM Journal on Imaging Sciences*, vol. 2, no. 1, pp. 183–202, 2009.

[21] R. Zdunek and A. Cichocki, "Improved M-FOCUSS algorithm with overlapping blocks for locally smooth sparse signals," *IEEE Trans. Signal Process.*, vol. 56, no. 10-1, pp. 4752–4761, 2008.

[22] J. A. Zhang, Z. Chen, P. Cheng, and X. Huang, "Multiple-measurement vector based implementation for single-measurement vector sparse bayesian learning with reduced complexity," *Signal Processing*, vol. 118, pp. 153 – 158, 2016.

[23] H. Duan, L. Yang, J. Fang, and H. Li, "Fast inverse-free sparse bayesian learning via relaxed evidence lower bound maximization," *IEEE Signal Processing Letters*, vol. 24, no. 6, pp. 774–778, 2017.

[24] S. Boyd, N. Parikh, E. Chu, B. Peleato, and J. Eckstein, "Distributed optimization and statistical learning via the alternating direction method of multipliers," *Found. Trends Mach. Learn.*, vol. 3, no. 1, p. 1–122, Jan. 2011.

[25] A. Gramfort, M. Kowalski, and M. Hämäläinen, "Mixed-norm estimates for the m/EEG inverse problem using accelerated gradient methods," *Physics in Medicine and Biology*, vol. 57, no. 7, pp. 1937–1961, mar 2012.

[26] B. E. Treeby and B. T. Cox, "k-Wave: MATLAB toolbox for the simulation and reconstruction of photoacoustic wave fields," *Journal of Biomedical Optics*, vol. 15, no. 2, pp. 1 – 12, 2010.

[27] P. van der Meulen, P. Kruizinga, J. G. Bosch, and G. Leus, "Coding mask design for single sensor ultrasound imaging," *IEEE Transactions on Computational Imaging*, vol. 6, pp. 358–373, 2020.

[28] T. Chernyakova and Y. Eldar, "Fourier domain beamforming: The path to compressed ultrasound imaging," *Ultrasonics, Ferroelectrics, and Frequency Control, IEEE Transactions on*, vol. 61, 07 2013.